Monolayer topography resolution achieved in a scanning near-field optical microscope

T. Plake, M. Ramsteiner,[a] and H. T. Grahn
Paul-Drude-Institut für Festkörperelektronik, Hausvogteiplatz 5-7, 10117 Berlin, Germany

(Received 15 July 2002; accepted 1 September 2002)

A low-temperature scanning near-field optical microscope has been adapted to achieve a high topographical sensitivity. This setup allows us to resolve morphological features on semiconductor surfaces of monolayer height, which is demonstrated for two different material systems, monolayer steps on an epitaxial GaN film and growth islands in a GaAs single quantum well (SQW) structure. Complementary photoluminescence measurements for the SQW structure reveal the potential of combining high-resolution topography with spatially resolved optical spectroscopy for investigating semiconductor nanostructures. © *2002 American Institute of Physics.* [DOI: 10.1063/1.1519936]

I. INTRODUCTION

With the growing interest in low-dimensional, nanoscale semiconductor heterostructures, there is a strong demand for high-resolution topographical and optical microscopy. In this respect, the scanning near-field optical microscope (SNOM) is an important tool, since it combines spatial resolution below the diffraction limit for optical spectroscopy with the feasibility to image topographical details by scanning force detection.[1,2] For optical, e.g., photoluminescence (PL), spectroscopy of semiconductor structures, cryogenic sample temperatures are often required. At the same time, the knowledge of very shallow morphological features on semiconductor surfaces is in many cases essential for the understanding of the optical properties.

The combination of shear-force and scanning near-field optical (NFO) microscopy has been well established.[3,4] There are several optical approaches to detect the damping of the NFO probe oscillation due to the probe–sample interaction and thus the probe–sample distance itself, among which are sophisticated interferometric implementations.[4] However, under cryogenic conditions, i.e., low temperatures and high vacuum, the use of nonoptical methods such as piezoelectric detection of the probe–sample interaction has been proven to be advantageous because of its simplicity.[5] This alternative method is based on quartz tuning forks, to which the NFO probe is attached. The probe–sample distance can be electrically monitored by the damping of the oscillator.

Recently,[6] the fundamental limits connected with the force detection using quartz tuning forks at atmospheric conditions and room temperature have been explored. In principle, the resolution is limited by the random motion of the prongs of the tuning fork due to thermal fluctuations resulting in a root-mean-square voltage noise of a few μV and hence the limit of a detectable displacement below 1 pm. This confirms earlier work, which deals with the minimum detectable displacement in shear-force sensors using a scheme based on diffracting a focused laser beam off the vibrating probe.[7] According to these results, a subnanometer vertical resolution (z direction) should be possible. Using optical dithering detection, Cricenti *et al.*[8] clearly achieved a z resolution below 1 nm using a multipurpose SNOM operating at room temperature and ambient pressure. However, for piezoelectric detection in a temperature-variable SNOM setup, such a high resolution is still a challenge, probably due to the increasing Q factor of the quartz tuning fork, which slows down the feedback loop when the temperature is lowered.

In this article, we introduce a low-temperature (LT) SNOM, which is based on a commercially available LT scanning tunneling microscope (STM). Using it in a shear-force detection mode, we achieved a very high topographical sensitivity, which enables us to resolve structures of monolayer (ML) height on surfaces of different materials such as GaN and GaAs. A comparison of the surface topography with spatially resolved PL measurements is performed for a GaAs single quantum well (SQW) structure to demonstrate the potential of this method.

II. EXPERIMENTAL SETUP

Our LT-SNOM is set up in a standard laboratory environment on an optical table with vibrational damping. Figure 1 shows a schematic of our system. A commercial LT-STM (Omicron) has been equipped with a large deflection piezo tube in order to achieve a scanning window of at least $10 \times 10\ \mu\mathrm{m}^2$ at cryogenic temperatures. All mechanical parts are arranged in such a way that the sample is mounted on an $x-y$ stage facing up, while the shear-force NFO scanner is separately attached to a z sledge. The coarse motion of the sample stage and the scanner sledge are implemented by ultrasonic drives. The microscope is inserted into a specially adapted continuous-flow He cryostat (Cryovac), which is equipped with a 10° tilted window to allow access to the sample by an external far-field collection lens.

Operating in a reflection geometry, we make use of two different configurations for NFO spectroscopy, *oblique illumination mode* and *illumination/collection mode*.[9] The latter one has the advantage that the lateral spatial resolution for

[a]Author to whom correspondence should be addressed; electronic mail: mer@pdi-berlin.de

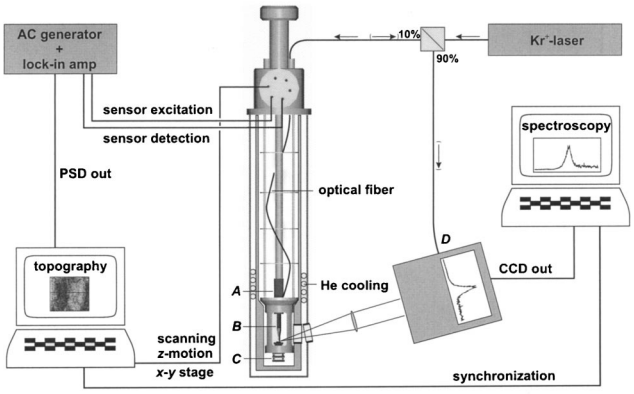

FIG. 1. Schematic diagram of the LT-SNOM setup. (Left) Shear-force topography mapping using a frequency generator for excitation of the tuning fork piezo and a lock-in amplifier for phase sensitive detection. (Center) Modified LT-STM in a cryostat including an ultrasonically driven *z*-slider (*A*), a large deflection scanning piezo tube with a tuning fork (*B*), and a $x-y$ sample stage (*C*). (Right) Acquisition of optical spectra by near-field measurements in two configurations (oblique illumination mode and illumination/collection mode). For the illumination/collection mode, a dichroic beam splitter (10% transmission, 90% reflection) is used, and the collected signal is guided to the fiber entrance (*D*) of the spectrograph.

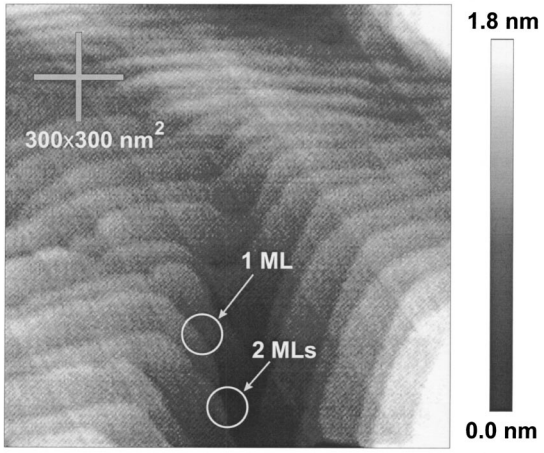

FIG. 2. Shear-force topography image of a GaN epitaxial film grown on a 6H−SiC substrate recorded at $T=300$ K. Mono- and bilayer steps are indicated by arrows (1 ML and 2 MLs, respectively).

PL scans is not limited by the diffusion of photoexcited carriers in the material. For the oblique illumination mode, we use factory-ready Al/Cr coated fiber probes (Nanonics) with apertures between 50 and 300 nm according to the experimental requirements. However, these probes are not suitable for the illumination/collection mode. In this case, we use uncoated tapered fiber probes, which we produce by a method called tube etching.[10] The illumination/collection mode yields a lateral resolution below 250 nm with a reasonable optical transmission, which was checked by measuring the PL intensity across a GaAs/(Al,Ga)As quantum wire structure.[11]

For optical excitation, the light of a Kr^+ laser passes through a dichroic beam splitter (10% transmission, 90% reflection), before it is coupled into an optical fiber and guided to the NFO probe. The emission from the sample can be collected either directly by a far-field collecting lens or through the NFO probe itself, from where it is guided back to the beam splitter and reflected into a second fiber coupler, which is connected with the fiber entrance of a spectrograph (Dilor Labram). The optical signal is dispersed by a 600 or 1800 lines/mm grating and detected by a charge-coupled device (CCD) array.

The control of the probe–sample distance is realized by shear-force detection using commercially available quartz tuning forks (typical resonance frequency of 32.7 kHz, 6 mm in length). The NFO probe is attached side by side to one of the prongs of the tuning fork using cyanacrylate superglue following the configuration of Karrai and Grober.[5] In contrast to the conventional configuration described in Ref. 5, we excite the oscillation of the tuning fork directly by applying a high-frequency voltage. The shear-force detection and topography mapping is realized by a lock-in amplifier with a built-in frequency generator. The phase shift between the driving sensor excitation and the detected quartz oscillation is converted into a dc signal, which is compared to the feedback set. During a NFO spectroscopy area scan, the stepwise movement of the NFO probe across the sample is triggered by the read out of the optical spectra from the CCD detector.

III. RESULTS

In the following subsections, we present two examples of high *z*-resolution topography mapping. First, we show that it is possible to observe features of only 0.3 nm height by mapping the inherent terrace-like patterns of monolayer steps in epitaxially grown GaN. Next, we present the topography of a GaAs/(Al,Ga)As quantum well (QW) structure, which reveals growth islands of monolayer height imaged at low temperatures. Finally, we demonstrate the potential of our setup by combining high-resolution topography with near-field optical experiments.

A. Monolayer steps on GaN

We investigated the surface topography of a hexagonal, 1-μm-thick GaN film deposited on a 6H−SiC substrate by plasma-assisted molecular-beam epitaxy (MBE).[12] The GaN *c* axis is oriented parallel to the growth direction. With its wurtzite crystal structure, the film can be viewed as a stack of two alternating GaN MLs, each of which has a step height of 0.26 nm. The sample surface commonly exhibits GaN ML terraces, which can be as wide as 200 nm.[13] The shear-force topography image of the GaN surface recorded at $T=300$ K is shown in Fig. 2. We can unambiguously identify curved and horizontally elongated features as steps of GaN MLs, while the diagonal stripes running across the image can be dismissed as artifacts, since they appear on different positions, when the scan is repeated. As indicated in the figure, we also observe that two ML terraces merge into one and hence form so-called bilayer steps, i.e., steps with a height of two GaN MLs, which are typical for this material. Figure 2 represents a high-quality topography image of a screw dislocation with a remarkable contrast—a result, which puts our shear-force SNOM in competition with atomic force microscopy (AFM) related techniques.

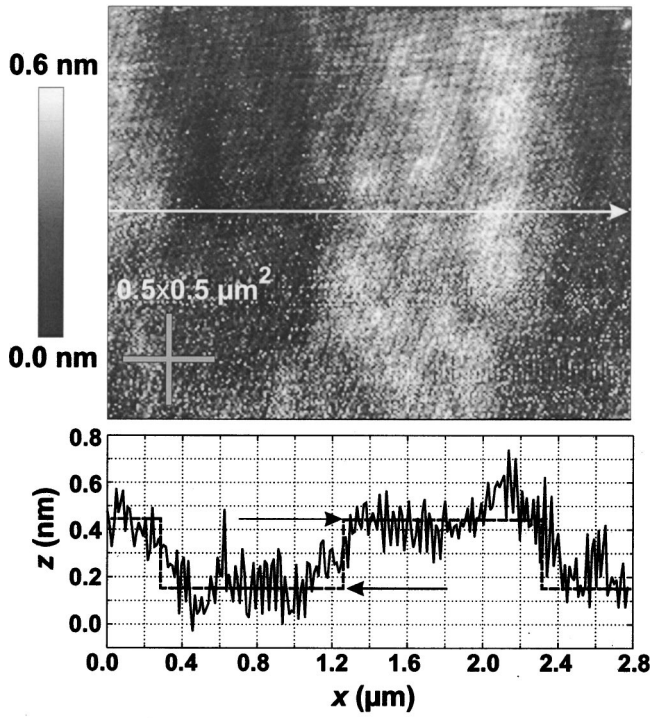

FIG. 3. Shear-force topography image of the sample surface of the GaAs SQW recorded at $T=13$ K. The line scan across the image (white arrow) shown on the bottom reveals a mean step height of 0.3 nm between two adjacent islands.

B. Monolayer fluctuations in quantum wells

1. Topography

We investigated the topography of a sample containing a GaAs SQW, which has been produced by solid-source MBE. It consists of a 5.4-nm-thick GaAs QW sandwiched between 1.13 nm/2.55 nm AlAs/GaAs superlattice (SL) barriers (20 periods on the substrate side and 4 periods on the surface side). The structure is capped with a 12 nm $Al_{0.5}G_{0.5}As$ and a 3 nm GaAs layer using the same growth conditions as for the SQW. The distance between the SQW and the sample surface amounts to 30 nm. At the SQW interfaces, the growth was interrupted for 120 s. In this way, the interfaces between the SQW and the SL barriers become particularly smooth, exhibiting large growth islands with a constant well thickness.

Figure 3 presents a high *z*-resolution topographical image of this SQW recorded at $T=13$ K. In the topography image, one can clearly identify two islands with a lateral diameter on the order of 1 μm in accordance with the expectations due to the applied growth conditions.[14] A line scan across the image reveals a mean step height of about 0.3 nm, which agrees very well with the thickness of one GaAs ML of 0.28 nm. The noise in the *z* direction was found to be below 0.1 nm at low temperatures. The typical island density was determined to be about 0.3 μm^{-2}, which was confirmed by AFM measurements.

2. Near-field optical measurements

In order to determine if the surface topography is connected to the morphology at the interfaces of the SQW, we recorded 26×26 NFO spectra in illumination/collection mode across a 3×3 μm^2 area at $T=13$ K. The excitation power was on the order of a few μW with a photon energy $E_{ex}=1.92$ eV. A typical PL spectrum is shown in Fig. 4, revealing three excitonic peaks at 1.626 (*A*), 1.635 (*B*), and 1.644 eV (*C*). This spectrum shows that the height fluctuations between these islands are typically 1 ML only in accordance with the design of the SQW and the assumption of ML fluctuations in the optical probing area.[15] The center line *B* dominates corresponding to the nominal SQW thickness with $n=19$ MLs. Hence, the high-energy peak *C* originates from islands with $(n-1)$ MLs, while the low-energy line *A* is due to islands with $(n+1)$ MLs.

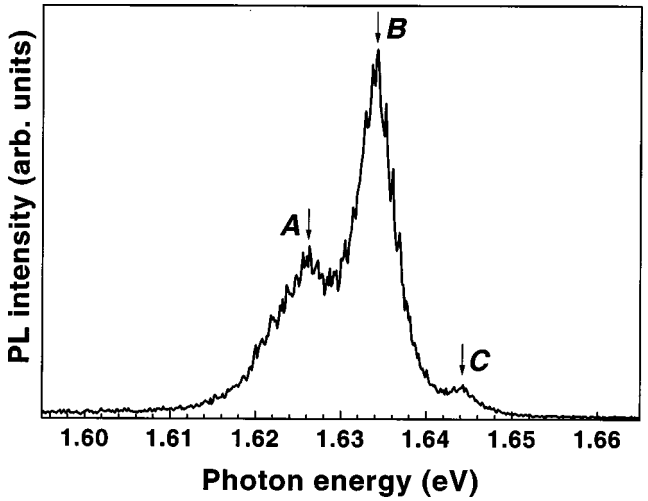

FIG. 4. PL spectrum of the GaAs SQW measured in near-field optical illumination/collection mode at $T=13$ K. Due to ML thickness fluctuations at both QW interfaces, the PL line is split into three bands at 1.626 (*A*), 1.635 (*B*), and 1.644 eV (*C*).

Figures 5(a), 5(b), and 5(c) depict NFO images of the PL intensities for the three ML-splitting peaks *A*, *B*, and *C*, respectively. The PL intensities are normalized to the total PL intensity of the spectrum. As expected, the NFO images of

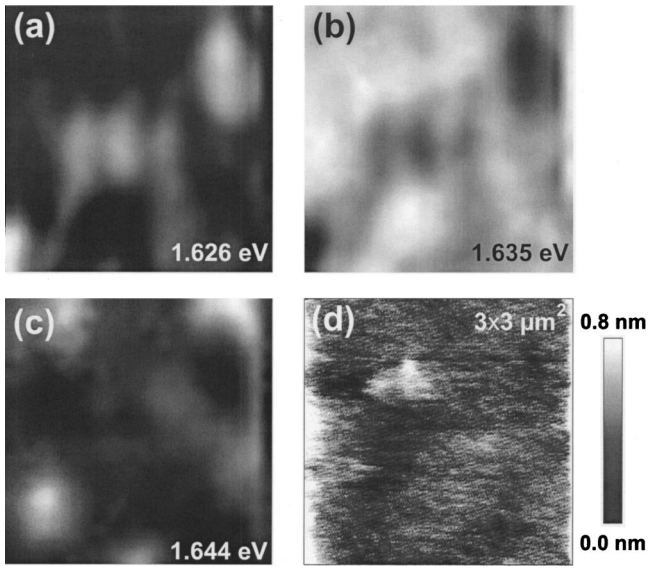

FIG. 5. NFO images of the PL peaks (a) *A*, (b) *B*, as well as (c) *C* in Fig. 4 of the GaAs SQW, and (d) the corresponding shear-force topography image recorded at $T=13$ K.

the three SQW PL lines are complementary to each other. For comparison, the surface topography for the same area scan, which was recorded first, is shown in Fig. 5(d). There is no direct spatial correlation of the islands between the topography of the sample surface in Fig. 5(d) and the PL intensity distributions in Figs. 5(a)–5(c). Consequently, we have to assume that the spatial location of the growth islands at the surface and SQW interfaces are uncorrelated.

An unintentional miscut of the GaAs substrate leads typically to epitaxial surfaces consisting of terraces and step edges. For terraces of lateral dimensions much larger than the diameter and distance of growth islands, the NFO images can be explained by a simple model assuming first an ideally flat QW region with a thickness of n MLs. Then, we add islands of 1 ML height on the lower or/and upper QW interface, resulting in areas with thicknesses of $(n-1)$, n, or $(n+1)$ MLs. On the basis of the surface topography image, we can simulate the spatial variation of the QW thickness for randomly distributed growth islands of about 1 μm diameter and a density of 0.3 μm^{-2} on both QW interfaces. For such a low density of growth islands, the NFO images of the PL peaks A [cf. Fig. 5(a)] and C [cf. Fig. 5(c)] essentially resemble the distribution of growth islands on the upper and lower QW interface, respectively. The resulting spatial thickness distribution corresponds to relative values of 48% for the center line B and 26% for both the low-energy and high-energy lines A and C, in reasonable agreement with the analysis of the NFO images in Figs. 5(a)–5(c). Thus, a coherent picture of the SQW interface structure is obtained by combining the surface topography with the optical results of the SQW obtained with our LT-SNOM setup.

ACKNOWLEDGMENTS

The authors gratefully acknowledge support by O. Brandt, R. Hey, and Y. J. Sun, who have provided the samples, and T. Hesjedal for helpful discussions.

[1] R. D. Grober, T. D. Harris, J. K. Trautman, and E. Betzig, Rev. Sci. Instrum. **65**, 626 (1994).
[2] H. F. Hess, E. Betzig, T. D. Harris, L. N. Pfeiffer, and K. W. West, Science **264**, 1740 (1994).
[3] E. Betzig, P. L. Finn, and J. S. Weiner, Appl. Phys. Lett. **60**, 2484 (1992).
[4] R. Toledo-Crow, P. C. Yang, Y. Chen, and M. Vaez-Iravani, Appl. Phys. Lett. **60**, 2957 (1992).
[5] K. Karrai and R. D. Grober, Appl. Phys. Lett. **66**, 1842 (1995).
[6] R. D. Grober *et al.*, Rev. Sci. Instrum. **71**, 2776 (2000).
[7] F. F. Froehlich and T. D. Milster, Appl. Phys. Lett. **65**, 2254 (1994).
[8] A. Cricenti, R. Generosi, C. Barchesi, M. Luce, and M. Rinaldi, Rev. Sci. Instrum. **69**, 3240 (1998).
[9] M. A. Paesler and P. J. Moyer, in *Near-field Optics* (Wiley, New York, 1996), p. 14.
[10] R. Stöckle, C. Fokas, V. Deckert, R. Zenobi, B. Sick, B. Hecht, and U. P. Wild, Appl. Phys. Lett. **75**, 160 (1999).
[11] R. Nötzel, M. Ramsteiner, J. Menniger, A. Trampert, H.-P. Schönherr, L. Däweritz, and K. H. Ploog, J. Appl. Phys. **80**, 4108 (1996).
[12] O. Brandt, R. Muralidharan, P. Waltereit, A. Thamm, A. Trampert, H. von Kiedrowski, and K. H. Ploog, Appl. Phys. Lett. **75**, 4019 (1999).
[13] A. Thamm, O. Brandt, Y. Takemura, A. Trampert, and K. H. Ploog, Appl. Phys. Lett. **75**, 944 (1999).
[14] R. Hey, I. Gorbunova, M. Ramsteiner, M. Wassermeier, L. Däweritz, and K. H. Ploog, J. Cryst. Growth **175/176**, 1167 (1997).
[15] M. A. Herman, D. Bimberg, and J. Christen, J. Appl. Phys. **70**, R1 (1991).